In-Situ Deformation of the Aortic Valve Interstitial Cell Nucleus Under Diastolic Loading

Hsiao-Ying Shadow Huang
Engineered Tissue Mechanics Laboratory,
Departments of Bioengineering
and Mechanical Engineering,
University of Pittsburgh,
Pittsburgh, PA 15219

Jun Liao

Michael S. Sacks[1]
Ph.D.
e-mail: msacks@pitt.edu

Engineered Tissue Mechanics Laboratory,
Department of Bioengineering,
University of Pittsburgh,
Pittsburgh, PA 15219

Within the aortic valve (AV) leaflet resides a population of interstitial cells (AVICs), which serve to maintain tissue structural integrity via protein synthesis and enzymatic degradation. AVICs are typically characterized as myofibroblasts, exhibit phenotypic plasticity, and may play an important role in valve pathophysiology. While it is known that AVICs can respond to mechanical stimuli in vitro, the level of in vivo AVIC deformation and its relation to local collagen fiber reorientation during the cardiac cycle remain unknown. In the present study, the deformation of AVICs was investigated using porcine AV glutaraldehyde fixed under 0–90 mm Hg *transvalvular pressures. The resulting change in nuclear aspect ratio (NAR) was used as an index of overall cellular strain, and dependencies on spatial location and pressure loading levels quantified. Local collagen fiber alignment in the same valves was also quantified using small angle light scattering. A tissue-level finite element (FE) model of an AVIC embedded in the AV extracellular matrix was also used explore the relation between AV tissue- and cellular-level deformations. Results indicated large, consistent increases in AVIC NAR with transvalvular pressure (e.g., from mean of 1.8 at* 0 mm Hg *to a mean of 4.8 at* 90 mm Hg*), as well as pronounced layer specific dependencies. Associated changes in collagen fiber alignment indicated that little AVIC deformation occurs with the large amount of fiber straightening for pressures below* ~1 mm Hg*, followed by substantial increases in AVIC NAR from* 4 mm Hg to 90 mm Hg*. While the tissue-level FE model was able to capture the qualitative response, it also underpredicted the extent of AVIC deformation. This result suggested that additional micromechanical and fiber-compaction effects occur at high pressure levels. The results of this study form the basis of understanding transvalvular pressure-mediated mechanotransduction within the native AV and first time quantitative data correlating AVIC nuclei deformation with AV tissue microstructure and deformation.* [DOI: 10.1115/1.2801670]

Keywords: extracellular matrix, fiber architecture, nucleus aspect ratio, finite element method, statistics

Introduction

Aortic valve (AV) leaflet interstitial cells (AVICs) are a heterogeneous group with characteristics of smooth muscle and fibroblasts (i.e., myofibroblasts). As the most numerous AV cell type, the AVIC population constitutes ~30% volumetric density in mice leaflets [1], and in AVIC isolated from human leaflets, ~78% expressed smooth muscle α-actin [2]. Their unique profiles of cell-cell and cell-ECM adhesion molecule expression [3,4], as well as the observation that age-related decreases in AVIC number accompany collagen fiber degeneration [5], suggest that AVICs are responsible for maintaining the valvular extracellular matrix (ECM). Recently, Merryman et al. [6] measured the stiffness of interstitial cells isolated from the leaflets of all four heart valves using micropipette aspiration and correlated it with smooth muscle α-actin and heat shock protein-47 (HSP47, a measure of collagen biosynthetic activity). Results suggested that interstitial cells respond to local tissue stress by altering cellular stiffness and biosynthetic levels.

At the tissue level, Chester et al. [7] exposed strips of AV leaflets to high KCl (90 mM) and endothelin levels under uniaxial tension, with both treatments generating modest force levels (circumferential direction: 0.31–0.66 mN, radial direction: 0.11–0.23 mN). From these results, it was speculated that these AVIC generated forces may subtly modulate leaflet motion during the opening/closing phases. Based on these novel findings, our laboratory utilized bidirectional flexure to reveal insights into how the AVIC population can alter native leaflet stiffness at the low strain levels experienced in bending [6]. These results indicated that changes in AVIC stiffness depended on bending direction and thus indicated layer specific behaviors. Further, a significant basal tone was observed and quantified for the first time. The results of both studies indicate that while the AVIC mechanical contribution to the leaflet tissue biomechanical behavior is negligible, AVICs are clearly tightly bonded to the surrounding ECM. As observed in vascular smooth muscle cells [8], we speculated that the contractile properties of AVICs are related to their role in managing ECM formation and strongly influenced by the local stress environments of the valve leaflet.

We have recently demonstrated that AV layers have substantially different mechanical properties, partly due to their different structures [9] and the presence of residual strains [10,11]. These results suggest that AVICs located in different layers may be exposed to different strains during the cardiac cycle. This led us to speculate that tissue-level structural changes observed under increasing transvalvular pressure (e.g., collagen fiber rotation, straightening, and compaction [9]) transduce concomitant strains to the embedded AVICs. Quantitative knowledge of how AVICs respond to tissue-level stress is thus a necessary step in understanding and modeling how organ level stresses are translated to cellular-level events. Yet, how the valvular tissue ECM strains are

[1]Corresponding author.

Contributed by the Bioengineering Division of ASME for publication in the JOURNAL OF BIOMECHANICAL ENGINEERING. Manuscript received September 3, 2006; final manuscript received April 19, 2007. Review conducted by Cheng Dong.

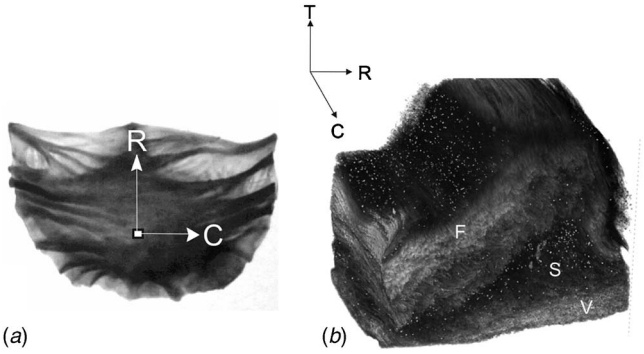

Fig. 1 (*a*) **An aortic valve leaflet showing gross structural features such as large surface undulations, along with the anatomical circumferential (*C*) and radial (*R*) axes. (*b*) A cross section of the AV leaflet 3D reconstructed to reveal the fibrosa (F), spongiosa (S), and ventricularis (V) layers, along with the 3D tissue coordinate system (*T* transmural)**

transmitted to the AVIC and the resulting deformations are, to date, unknown. These considerations led us to hypothesize that AVIC deformations might provide key insight into a broad spectrum of questions related to cell/ECM interactions, including but not limited to mechanisms of native AV homeostasis and pathophysiologic degeneration. A first step in these goals is the quantification of AVIC deformations in the native valve.

In the present study, we investigated the relationship between quasi-static physiological levels of transvalvular pressure and AVIC deformation. This was accomplished by analyzing histological sections taken from porcine aortic heart valves fixed under varying controlled pressures [9]. Since the deformation of a complete cell (i.e., membrane, cytoplasm, and nucleus) within intact tissues is complex and not fully understood, we choose to utilize the change in AVIC nuclear aspect ratio (NAR) as an index of overall cellular deformation. We also quantified the distribution of AVIC NAR in each layer. Finally, we performed finite element (FE) simulations incorporating AVIC/ECM interactions to gain insight into how the mechanical behavior of native AV leaflet tissues is linked to AVIC deformation.

Methods

Histological Preparation and Database. All tissue sections were taken from a previous study by Sacks et al. [9], where methods have been fully described. In brief, fresh porcine aortic heart valves were shipped in chilled physiological saline, and the aortic root-valve complex was removed immediately upon arrival. Care was taken to remove as much of surrounding myocardium as possible from the root area, and the coronary arteries were closed with sutures. After this preparation, each AV was mounted into a device that allowed for a steady pressure head while the valves were fixed at a preset transvalvular pressure level. The device was then flooded with a fixative solution consisting of 0.5% glutaraldehyde in phosphate buffered saline (PBS), in which the AV was complete submersed. In order to provide physiological loading to aortic valve, tissue pairs of valves were fixed at pressures of 0 mm Hg (i.e., free floating), 1 mm Hg, 2 mm Hg, 4 mm Hg, 60 mm Hg, and 90 mm Hg, yielding a total of six leaflets per pressure level. After fixation, the collagen architecture of each AV leaflet was quantified using small angle light scattering (SALS). Next, rectangular (1×4 mm^2) tissue sections were dissected from the central belly region oriented with their long dimension parallel to the circumferential axis (Fig. 1), which is coincident with the collagen fiber preferred direction. The specimens were stained using hematoxylin and eosin (HE) or Masson methods. A total of 48 slides were assessed for all transvalvular pressure levels.

An advantage of using the specimens from our previous study [9] is that it allowed direction quantitative comparisons between changes in AVIC NAR with collagen fiber alignment. To simplify the present analysis, we converted the previous orientation index (OI) to a normalized orientation index (NOI) scale as follows. The OI is defined as an angular width that contained 50% of all fibers [12,13]. Since the upper bound of the OI is 90 deg for a completely random fiber network, the NOI is defined here NOI $=(90\ \text{deg}-\text{OI})/90$ deg. Thus, a NOI of 1 indicated that the collagen fibers in the tissue were perfectly aligned and a NOI of 0 indicated completely random fiber alignment.

Histological Section Imaging. The valve anatomical directions, circumferential (*C*), radial (*R*), and transmural (*T*) axes were used for the local coordinates in all specimen (Fig. 1). Each histological slide contained three sequentially cut sections cut in the *C-T* plane (Fig. 1(*b*)). Five overlapping photomicrographs ($400\times$ magnification, 1 pixel$=0.4$ μm) covering the complete thickness (including three leaflet layers: fibrosa, spongiosa, and ventricularis) were obtained (Fig. 2, Table 1). In addition to the 2D histological sections, we also utilized a representative digital volumetric image (DVI) of a 1×1 mm^2 section taken from a porcine aortic valve fixed at 0 mm Hg from the central belly region (Fig. 1(*b*)). This was done to provide radial-transmural cross-sectional supplementary information for three-dimensional computations of nuclear geometry. The DVI image was prepared through visualization and analysis software RESVIEW 3.2 (Resolution Sciences Corporation, Corte Madero, CA) and provided a digital three-dimensional virtual replica of the native aortic valve tissue sample. Details of this approach have been presented in Gloeckner [14].

Image Processing. All AVIC nuclear dimensions were quantified from the photomicrographs along the transmural (*C-T* plane) plane. Since the view range of the microscope was limited, a panoramic image was required to cover all three layers. In order to achieve the best quality for panorama image generation, 50–70% range of overlapping was required along the transmural direction; detailed imaging methods were described by Engelmayr et al. [15]. A total of 720 panoramic photomicrographs were digitized resulting in 142,560 AVIC nuclear geometries acquired (Table 1).

From the 3D DVI images, we noted that elliptic AVIC nuclei of the histological sections we utilized were consistently observed to lie within the *C-R* plane (Fig. 1(*b*)) and were generally aligned near the *C-T* axis (Fig. 2(*b*)). Since the AVIC nuclei were often observed sectioned offset from their centroid (Fig. 2(*b*)), direct usage of dimensional measurements would not lead to meaningful results. However, since AVIC nuclei were observed to be aligned to the *C-R* plane, the aspect ratio of elliptical sections taken orthogonal to the long axis will be maintained regardless of section plane orientation. Thus, the AVIC NAR was chosen as a two-dimensional measurement of nucleus shape rather than the unidimensional values of absolute nucleus length and width alone.

The major and minor axis lengths of the deformed AVIC nuclei were quantified using SigmaScan (SPSS, Inc., Chicago, IL) (Fig. 2(*b*)). In addition, based on the available AVIC NAR data in the *C-T* (measured from the histological sections) and the *C-R* planes (measured in the DVI data for 0 mm Hg only), we utilized an ellipsoidal nuclear geometry, in which *a*, *b*, and *c* were the major axis lengths in the circumferential, radial, and transmural directions (Fig. 1(*b*)). Assuming incompressibility, we converted the *C-T* NAR data to overall changes in nuclear geometry. Finally, in order to correlate the relationship between the valve tissue layer and cellular deformation, the AVIC nucleus spatial location in the transmural direction was determined and expressed as a normalized thickness.

Statistical Analyses. Statistical comparisons were performed to correlate the effects of transvalvular pressure on AVIC nuclear geometry from the available histological specimen database (Table 1). All statistical data analyses were performed using SYS-

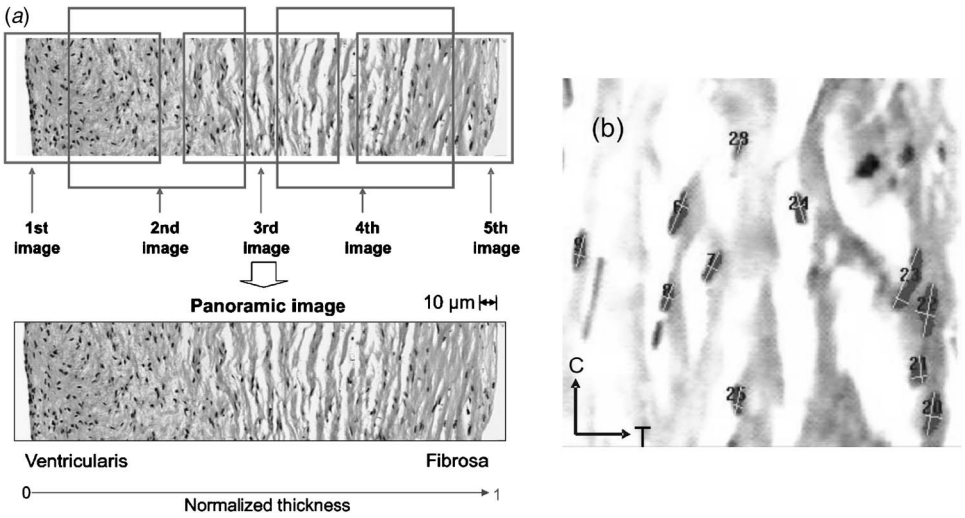

Fig. 2 (*a*) **A panoramic image was created from four to five overlapped images of histological sections in order to span all three AV leaflet layers.** (*b*) **A representative image of AVIC nuclei (highlighted red) within Masson's stained AV tissue section. The major- and minor-axis lengths used in calculated NAR are identified (yellow lines). The *C-T* coordinates of the nuclei centroids were computed and converted to a normalized thickness position, with the origin arbitrarily defined at the ventricular surface.**

TAT (SYSTAT 10, SPSS, Inc., Chicago, IL) through an analysis of variance (ANOVA) method. Differences between measures were deemed significant when $p<0.05$. Details of the statistical analyses can be found in Huang [16].

Finite Element Simulations of Aortic Valve Interstitial Cell Nuclear Aspect Ratio. In addition to performing experimental studies, we also sought to gain insight into how mechanical forces and deformations are transmitted from the AV leaflet tissue to the AVIC by developing the following tissue-level model. A two-dimensional finite element model of the central region of the AV leaflet was developed, wherein in a small representative volume element (RVE) of the lower belly region of the leaflet was simulated (Fig. 3). First, in order to apply physiological loads to the RVE model, we assumed that the central region of the AV leaflet was spheroidal (radius ~10 mm [17]), so that transvalvular pressures applied to the valvular model could be transformed into a local biaxial tension states through the Laplace law (Fig. 3(*a*)). Thus, for a transvalvular pressure (TVP) of ~90 mm Hg the resulting tension is $T=60$ N/m. This value corresponds to the peak physiological tissue stress of 120 kPa in the belly region assuming a thickness of 0.5 mm [18,19]. An equibiaxial loading state was applied at the boundaries, using an equivalent force of 0.6 N.

Though leaflet is composed of multiple layers, for simplicity the leaflet was modeled as a single layer (representing the fibrosa). We assumed that the size of the RVE model [20,21] is relatively small such that model contains only one VIC nucleus and surrounded by the ECM, as justified by the spatial distribution of AVICs in the leaflet (Fig. 2(*b*)). Specifically, we chose the dimensions of the RVE model to be 100 μm × 100 μm × 0.5 mm, with the thickness based on available data [10]. The AVIC/nucleus was simulated as a single phase ellipsoidal inclusion, with the AVIC nucleus/ECM boundary assumed to be perfectly bonded, i.e., displacements are continuous over the edge of the VIC nucleus. To specify the AVIC nucleus shape, we noted that at 0 mm Hg pressure an average AVIC NAR of 1.8 was observed in the *C-T* plane. Utilizing an ellipsoidal geometry and assuming incompressibility as noted above, we computed an AVIC NAR of 1.35 in the *R-C* direction. Thus, we modeled the elliptic AVIC nucleus with dimensions 7.5 μm in the radial direction (set as a reference length) and 9.75 μm in the circumferential direction (Fig. 3(*b*)). Eight-node quadrilateral and six-node triangle reduced-integration plane-stress elements were used in the RVE model with number of 1674 elements (Fig. 3(*b*)).

Assignment of the material model and mechanical properties for the tissue and AVIC nucleus were determined as follows. For the tissue, we utilized a structural constitutive model and material parameters for the native aortic valve leaflet [22]. Details of the FE implementation of the structural constitutive model have been recently presented [23]. Although the FE model was originally formulated to utilize a fiber recruitment model, for the present study, we utilized the "effective" exponential collagen fiber model [22] to simplify computations.

Currently, we do not have direct measurements of the AVIC nucleus mechanical properties. We have recently estimated the effective elastic modulus E of all heart valves interstitial cells using the micropipet aspiration technique [6]. Under the assumption of incompressible linear elasticity [24], effective mean modulus of 0.449 ± 0.024 kPa was obtained. This model assumed the cell to be a homogeneous material while ignoring discontinuities (organelles, nucleus, etc.) and viscous effects from the cytosol. In the present model, to account for large deformations we thus choose a neo-Hookean hyperelastic material with $G=0.4$ kPa fol-

Table 1 Summary of histological specimen database

							Total
Pressure level (mm Hg)	0	1	2	4	60	90	6
Number of slides per pressure	8	8	8	8	8	8	48
Number of sections per slide	3	3	3	3	3	3	144
Number of images per section	5	5	5	5	5	5	720
Number of cells per image	152	245	133	175	224	259	142,560

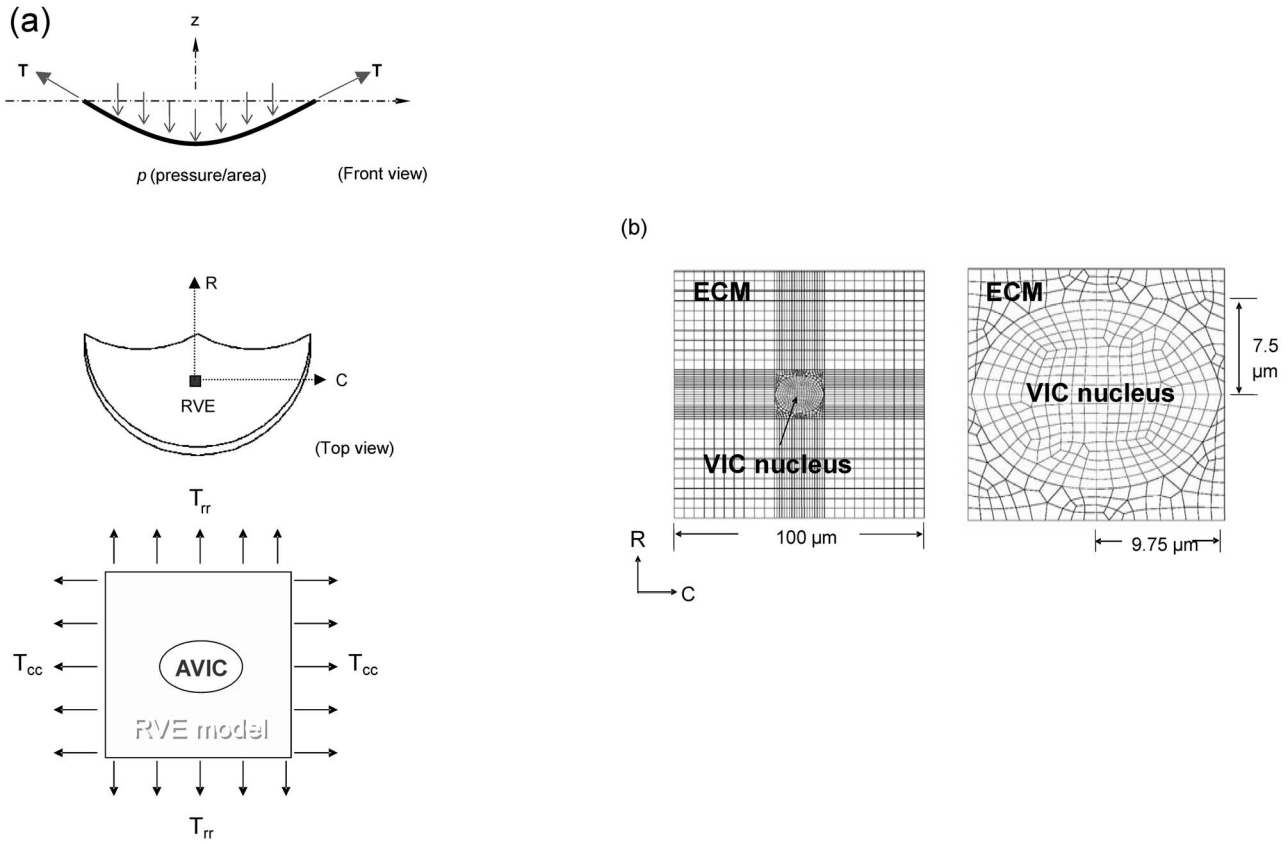

Fig. 3 (*a*) **Schematic illustrating an AV leaflet subjected to a uniform tension *T* at the edge and a uniform pressure *p*. The model boundary stresses for the RVE were based on the applied external tensions *T*, and were located at the center of the leaflet.** (*b*) **The FE mesh consisting of an AVIC nucleus within leaflet ECM (cell membrane and cytoplasm were considered negligible).**

lowing Baer et al. [25]. Parametric studies of various AVIC nuclei material properties were also conducted, which included a linear elastic homogenous isotropic (LEHI), similar to Baer et al. [25,26]. Following Baer et al., we assumed for the LEHI AVIC nuclei model an elastic moduli of 9×10^{-4} MPa, which was also varied by $\pm$ two magnitude orders.

The final displacements in the circumferential and radial directions of the deformed AVIC nuclei under 1 mm Hg, 2 mm Hg, 4 mm Hg, 60 mm Hg, and 90 mm Hg were generated from the finite element solver (ABAQUS 6.3, Hibbitt, Karlsson & Sorensen, Inc., Pawtucket, RI). Final major axis lengths were then calculated through determined displacements. Circumferential and radial stretches, λ_1 and λ_2, were calculated from the final major axis lengths divided by the original major axis lengths, and λ_3 was calculated by using the incompressibility assumption (i.e., $\lambda_3 = 1/(\lambda_1\lambda_2)$). The predicted AVIC NARs in the circumferential-transmural directions were then calculated by a/c, in which a and c were defined previously.

Transmission Electron Microscopy. To demonstrate connectivity between the AVIC membrane and surrounding ECM, specimens of AV were prepared for TEM using methods similar to a previous study [27]. Specimens were fixed with 2.5% glutaraldehyde, trimmed to a length of 1 mm, postfixed with 1% osmium tetroxide (1 h), 1% uranyl acetate in maleate buffer (1 h), and dehydrated with graduated concentration of ethanol and propylene oxide. Specimens were then infiltrated and embedded in epon (polymerized at 60°C for 48 h). Ultrathin sections (85 nm thick) were cut using an ultramicrotome (Reichert Ultracut; Leica Microsystems GmbH, Wetzlar, Germany) mounted on uncoated grids, and stained with uranyl acetate and lead citrate. Specimens were then observed with a JEOL 1210 TEM (JEOL USA, Inc., Peabody, MA).

Results

Aortic Valve Interstitial Cell Nuclear Aspect Ratio Transmural Variations. To delineate layer variations, the AVIC NAR were plotted against normalized leaflet thickness (Fig. 4(*a*)). Generally, TVP level was found to have a significant effect on NAR values. At 0 mm Hg, the AVIC NAR maintained a constant transmural value of ~1.8. In the fibrosa layer (normalized thickness range from ~0.4 to 1), the AVIC NAR at 4 mm Hg slightly increased. Under peak physiological TVP (90 mm Hg), the AVIC NAR were not only substantially greater than at low-pressure levels but also demonstrated substantial transmural variations. In particular, the NAR exhibited greater increases in the fibrosa layer (~4.8 compared to ~3.0 for the ventricularis layer, Fig. 4(*a*)), which were statistically larger than both the corresponding 90 mm Hg ventricularis and lower pressure NAR values ($p < 0.05$).

The Relationship Between Nuclear Aspect Ratio and Collagen Fiber Architecture. An overall positive trend was found between the AVIC NAR and the degree of collagen fiber alignment as quantified by the NOI (Fig. 4(*b*)). Rather than observing a simple relationship, we instead noted the following three distinct regions (Fig. 4(*b*)):

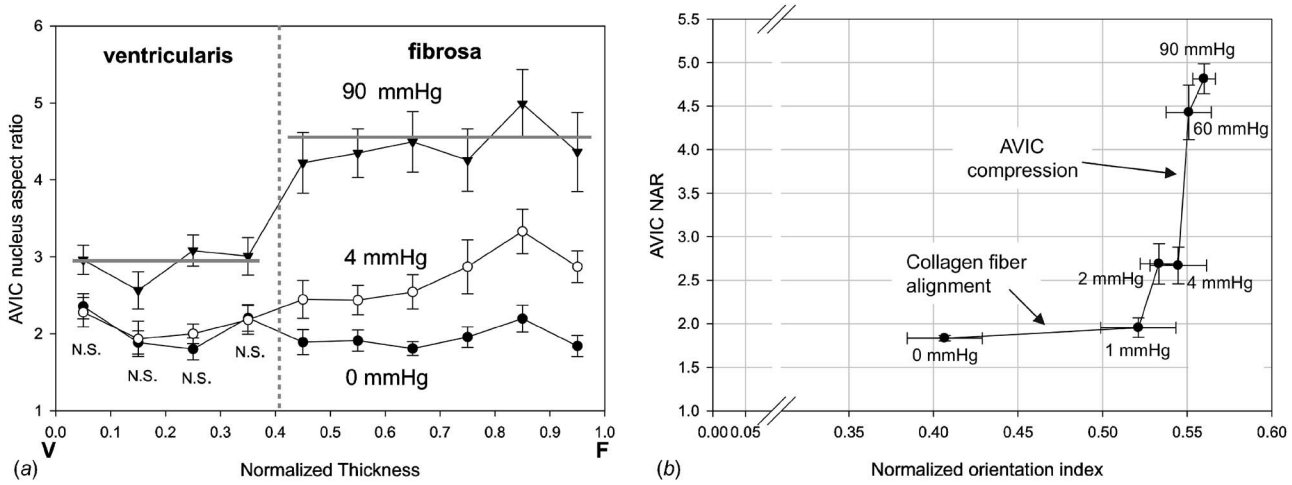

Fig. 4 (*a*) **AVIC NAR versus normalized thickness at zero-, low- and high-TVP levels. At 0 mm Hg TVP, AVIC NAR values were highly uniform across the entire leaflet thickness. For normalized thickness positions between 0 and 0.3 (i.e., within the ventricularis layer), AVIC exhibited similar NAR values of ~2.2 (0 mm Hg and 4 mm Hg) and ~3 (90 mm Hg). In sharp contrast, for normalized thickness positions between 0.4 and 1 (i.e., within the fibrosa layer) the AVIC NAR exhibited a trend of increased value with increased thickness position, approaching an average value of ~4.8 at 90 mm Hg. These data indicate that AVICs in the different leaflet layers are subjected to dramatically different external stresses. "N.S." indicates no statistically significant differences. (*b*) Comparison of the mean transmural AVIC NAR with the NOI (a measure of the degree of collagen fiber orientation). A complex relationship consisting of three distinct regions was observed (see text for details).**

1. An initial region characterized by a large change in collagen fiber alignment and little change in AVIC NAR between 0 mm Hg and 1 mm Hg.
2. A transition region between 1 mm Hg and 4 mm Hg associated with modest changes in both parameters.
3. A steep region between 4 mm Hg and 90 mm Hg associated with a large increase in AVIC NAR but small changes in collagen fiber alignment.

Due to the observed transmural variations (Fig. 4(*a*)), we subdivided the AVIC NAR results into the ventricularis and fibrosa layers, setting the boundary between both layers to be at ~0.35 normalized thickness based on recent data [10] (Fig. 5). Although both responses were qualitatively similar, the fibrosa demonstrated a substantially greater rate of NAR change over a smaller range of NOI (Fig. 5) compared to the ventricularis layer. Specifically, the AVIC NAR at 0 mm Hg in the fibrosa and ventricularis were approximately equal (NAR ~2), and that NOI at 0 mm Hg of the fibrosa layer was significantly larger than one of the ventricularis layer (~0.463 versus 0.355). Furthermore, the AVIC NAR observed under 90 mm Hg was significantly higher in the fibrosa compared with the ventricularis (~5 versus ~4).

To facilitate visualization of the above NAR data, we utilized the measured mean nuclear dimensions and computed the transmural direction based on the incompressibility assumption. The mildly ellipsoidal shape of the AVIC NAR at 0 mm Hg can be readily observed (Fig. 6(*a*)). Under 90 mm Hg, the substantial deformations of the AVIC nucleus can be observed (Fig. 6(*b*)). Nuclear dimensional changes were greatest in the radial direction, consistent with the larger tissue strains in this direction [18,19].

Finite Element Model Simulations. The peak stretches at the

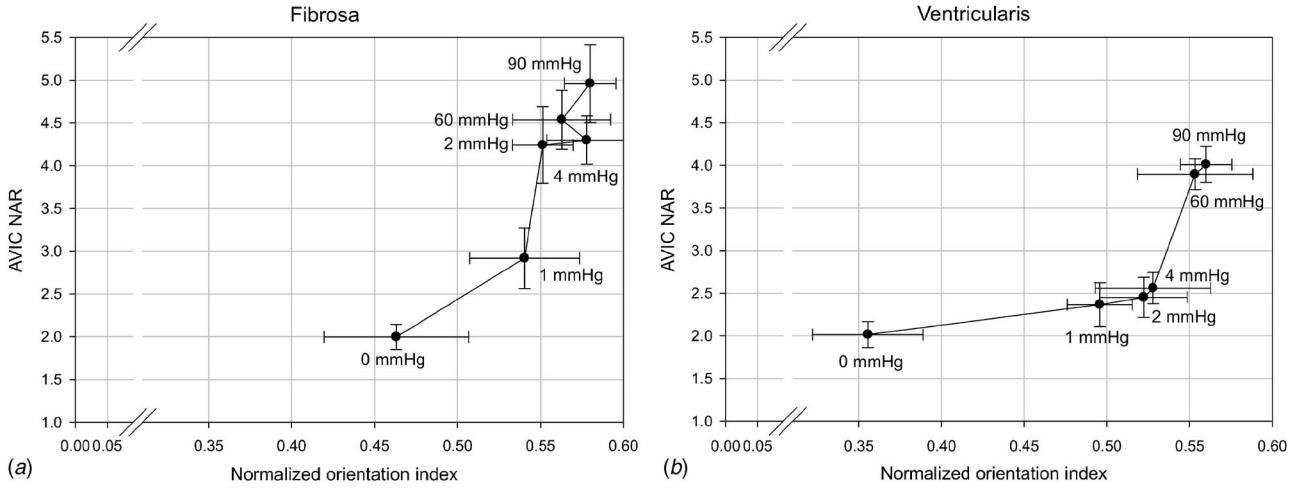

Fig. 5 AVIC NAR versus NOI in the ventricularis and fibrosa layers for all TVP levels. Although both responses were qualitatively similar, the ventricularis underwent overall larger changes in NOI but lower changes in NAR. The fibrosa layer demonstrated a greater NAR change over a smaller range of NOI compared to the ventricularis layer, and the maximum NAR was significantly higher in the fibrosa compared with the ventricularis (~5 versus ~4), suggesting that the AVICs in this layer are more highly compressed.

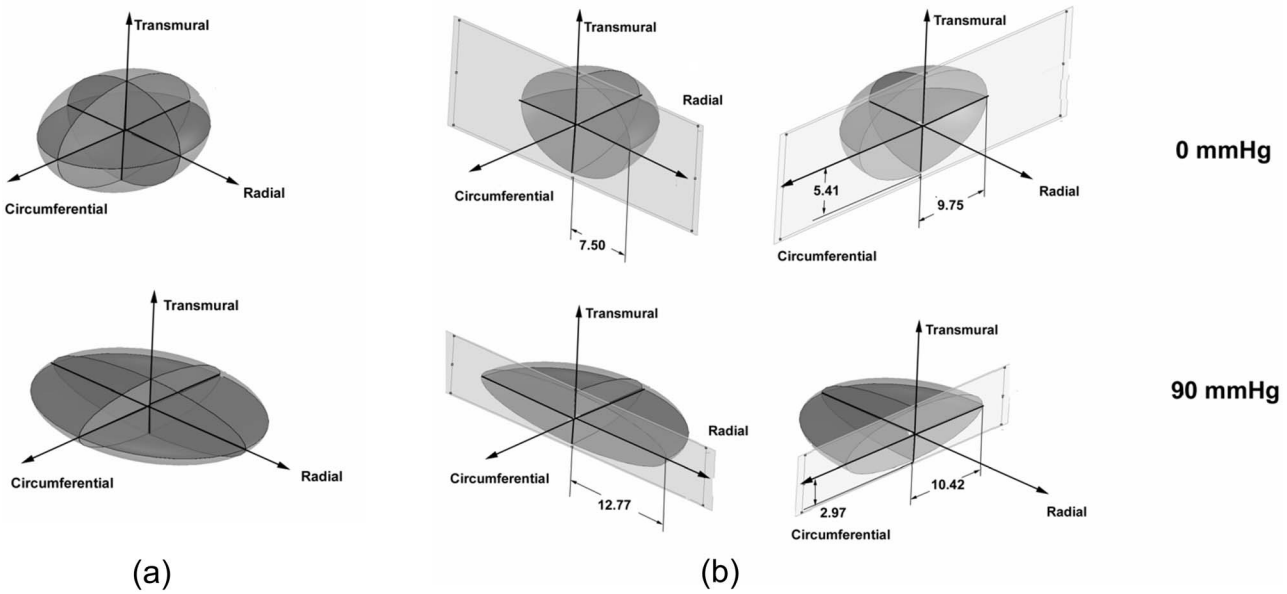

Fig. 6 Schematic representations of AVIC nucleus geometry at (*a*) 0 mm Hg and (*b*) 90 mm Hg. Deformations of the AVIC nucleus at 90 mm Hg in the circumferential and radial directions were taken from our experimental data, with the transmural dimensions calculated based on an incompressibility assumption. Although similar to valvular tissue-level deformations, AVIC nuclei experienced greater dimensional changes due to a disparity in mechanical properties compared to the leaflet ECM.

interface if the AVIC nucleus/ECM to the stretches at the model boundary (Fig. 3(*b*)) indicated that peak stretches at the interface were 1.053 compared to 1.014 at the boundary and 1.655 compared to 1.500 at the boundary for the circumferential and radial directions, respectively. Thus, the presence of the AVIC significantly affects the local tissue deformation (under the continuum material assumption), and demonstrate how the large disparity in AVIC nuclei and ECM stiffness result in nuclei deformations that do not simply follow local tissue strains. Moreover, local strain distributions indicated local effects of the AVIC in a region of 1–2 cell diameters (see details in Huang [16]). Given that the apparent cell density of the valvular ECM appears to indicate a mean intercell distance of greater than 2 cell diameters, (Fig. 2(*b*)), we feel that this result lends support to our model geometry (Fig. 3(*b*)).

When compared to the measured AVIC NAR, the FE model captured the overall trends of the relation between AVIC NAR and TVP (Fig. 7(*a*)). However, while good agreement was found for 0 mm Hg and 1 mm Hg (Fig. 7(*a*)), the results for 2–4 mm Hg pressure levels underestimated the NAR values by ~0.5. Larger discrepancies were observed at higher pressures of 60–90 mm Hg, with accompanying errors of ~1.0. Parametric studies of various AVIC nuclei material properties indicated that even with these large ranges of mechanical properties, all models exhibited similar behavior (Fig. 7(*b*)). This is not a surprising result in light of the substantially stiffer valvular ECM.

Discussion

Study Overview. The present study is the first known to the authors to systematically examine the deformation of the valvular interstitial cells within the leaflet under a physiological range of

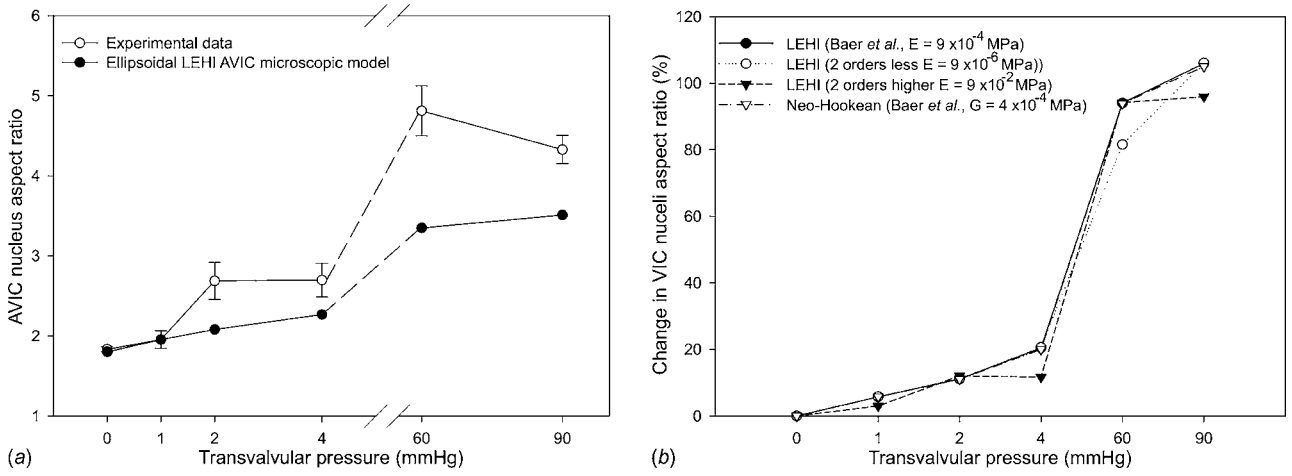

Fig. 7 (*a*) A comparison of experimentally measured AVIC NAR values with values predicted by the RVE model plotted against the experimentally applied levels of TVP. While the RVE model captured the overall trend, discrepancies with the experimental data increased at greater TVPs. (*b*) Model predicted data as a function of material stiffness, indicating insensitivity to the material model.

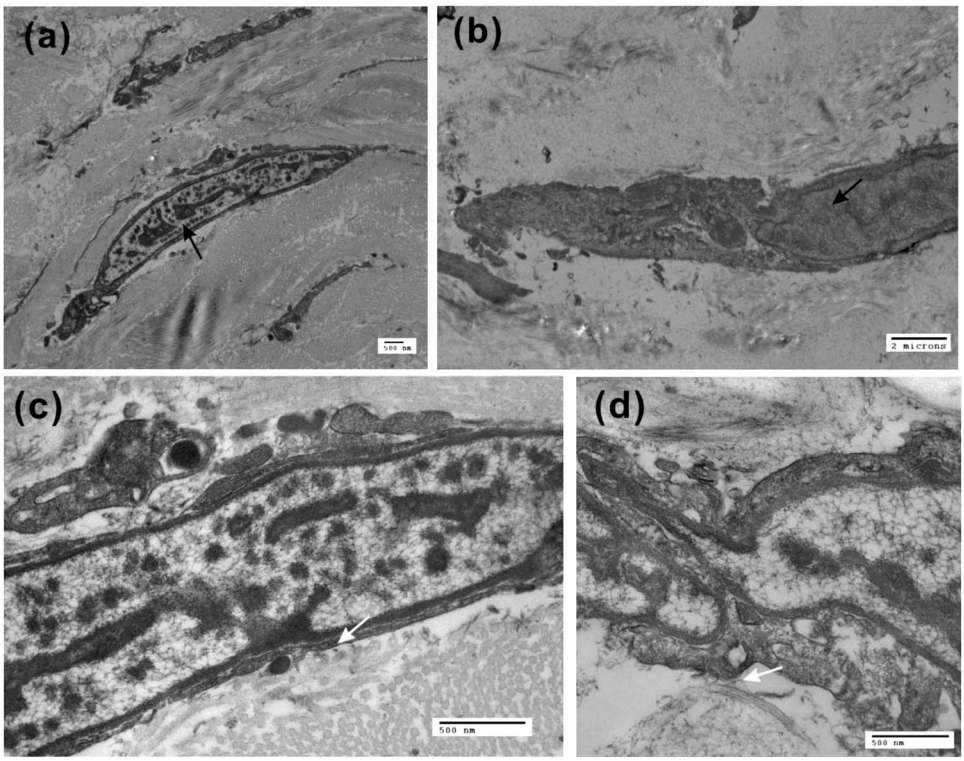

Fig. 8 TEM images of intact AVIC within the leaflet ECM. (*a, b*) Overall morphology of cell-ECM integration. Cell nucleus is indicated by a black arrow. (*c, d*) connections between collagen fibrils and cell membrane highlighted by white arrows. Scale bars=2 μm in (*b*) and 500 nm (*a, c* and *d*).

TVPs. The NAR was used as an index for gauging cellular deformations, for which related studies support. For example, Knight et al. [28] observed that the deformations of compressed chondrocytes were associated with the deformations of their nuclei. They also concluded that the nucleus was stiffer than the surrounding cytoplasm, suggesting that nuclear deformation was representative of the overall chondrocyte deformation. Peeters et al. [29] found that myoblasts and myoblast nuclei deformed preferably in the same direction, suggesting that structural restrictions to overall cell deformation (e.g., the actin cytoskeleton) may also apply to the cell nucleus.

While it is axiomatic that tissue-induced cellular deformations are involved in regulating cellular mechanobiological responses, actual in vivo cellular deformations are very tissue specific. For example, Screen et al. [30] measured tenocyte NARs in situ via confocal microscopy of digital extensor tendon fascicles fluorescently labeled for cell nuclei. They reported higher NAR values than those observed in the current study (e.g., ranging from ~3.5 at 0% strain to ~5.25 at 5% uniaxial strain). They also found lower changes in tenocyte normalized NAR with applied strain (~1.8-fold average change compared to 2–2.5-fold average change reported in the present study). This is likely due to the much lower tissue strains that typically occur in the tendon compared to heart valve leaflets, which are also subjected to a biaxial stress state. Both the previous and current studies underscore the need to perform cell/tissue specific measurements.

An important assumption in the present study was that the AVIC are tightly bound to the local ECM. While direct measurements of AVIC-ECM adhesion strength do not presently exist, the principal adhesion molecules associated with AVIC-ECM interactions have recently been elucidated (i.e., $\alpha_2\beta_1$ and $\alpha_3\beta_1$ integrins [3]), and AVICs are known to be capable of producing measurable tissue-level forces [7,31,32], suggesting that AVICs are tightly bound to the leaflet ECM. To help provide insight into AVIC/ECM interactions, we obtained TEM images of porcine AV interstitial cells (Fig. 8). We found that that the AVICs were closely integrated with the ECM, suggesting that ECM deformations are readily transformed to AVIC via direct contact and mechanical interactions. While it is not known how the resulting ECM deformations are passed to the AVIC nuclei by the AVIC cytoskeleton network, the large nuclear deformations observed in the present study suggest that the AVIC cytoskeleton network is relatively stiff and that nuclear deformations are a good index of overall AVIC deformation.

Aortic Valve Interstitial Cell Aspect Ratio/Leaflet Extracellular Matrix Mechanical Interactions. An important observation of the present study was the nonlinear relationship between AVIC NAR and collagen fiber alignment (as quantified by the NOI) (Fig. 4(*b*)). Given the complex tissue microstructure found in collagenous tissues [33,34], this is not a surprising result. In particular, collagen fiber crimp common to all collagenous tissues will likely induce a nonhomogeneous strain field within the tissue. Yet, the three-phase response observed for the AV leaflet (Fig. 4(*b*)) suggests additional mechanisms likely play a role.

Specific insights into the AVIC/ECM micromechanical interactions can be inferred from the AVIC NAR-NOI relation (Fig. 4(*b*)), which are summarized in Fig. 9. First, we observed substantial increases in NOI (i.e., large increases in fiber alignment) with little change in AVIC NARs for 0 mm Hg to 1 mm Hg TVPs. Here, as the constituent fibers straighten primarily via rotation under strain (inducing an increase in NOI), there is little direct influence on the AVIC. Thus, AVICs may be simply moved in a rigid body like fashion during the initial reorganization of the ECM constituents as the leaflet tissue is initially stretched. Next, at the 1–4 mm Hg pressure levels, there are small changes in NOI with increased measured AVIC NAR. This suggests that only once the collagen fibers straighten do the AVICs initially begin to de-

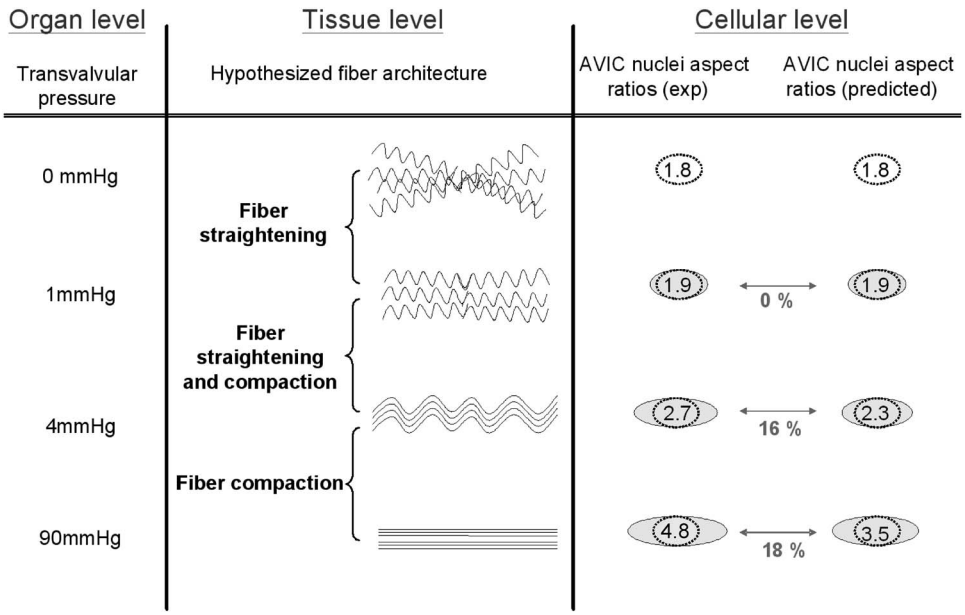

Fig. 9 A summary schematic depicting fiber straightening and compaction effects with corresponding AVIC nuclei deformation. The percent error between the experimental data and model predictions is indicated.

form. Next, we know that the AV collagen fibers are mostly straightened at ~4 mm Hg [9,35,36], with only minimal changes in collagen alignment at greater pressures. Yet, the greatest changes in AVIC NAR occurred at pressures above 4 mm Hg. Thus, continued deformation of the AVIC nucleus was likely due to fiber-compaction effects that occur only when the collagen fibers are fully straightened when the valve leaflets are coapted.

Layer Specific Responses. Although starting from the same initial geometric state at 0 mm Hg TVP, at all subsequent pressure levels, the AVIC NAR was higher in the fibrosa compared to the ventricularis (Figs. 4 and 5). This may be due to substantial difference in the layer mechanical properties [10], which result due to the high elastin content and prestretch of the ventricularis [35,37]. The high elastin content may serve to dampen the coupling between the AVIC/ECM. Yet, at TVPs $\geqslant$60 mm Hg, both layers exhibited similar total effective collagen fiber alignment (i.e., similar NOI values [9]), yet demonstrated different AVIC NAR values (Fig. 5). This result suggests that other factors, such as the local collagen fiber density and the specific microarchitectures of the leaflet layers (Fig. 6), may play a role in altering the local AVIC microenvironment.

Finite Element Simulations: The Effects of Aortic Valve Interstitial Cell Boundary Conditions and Mechanical Properties. In the present study, we choose a neo-Hookean mechanical property model for the AVIC nucleus. Overall, this model predicted the trend of measured AVIC NARs (Fig. 7(*b*)). This result supports the assumption of tight coupling to the surrounding ECM, in agreement with previous studies [38] and the TEM results (Fig. 6). However, we did not explicitly model the AVIC cell membrane and cytoplasm. Atomic force microscopy (AFM) results recently performed in our laboratory on AVICs [39] indicated that the cell stiffness immediately over the nucleus was on average 3.5 times stiffer than the periphery of the cell. Moreover, the FE model appeared to be insensitive to AVIC nuclear mechanical properties, which is not surprising given the large disparity between AVIC and ECM stiffnesses. Related studies demonstrated similar trends, such as the work by Guilak et al. [40] who estimated the viscoelastic properties of mechanically and chemically isolated nuclei of articular chondrocytes using micropipet aspiration in conjunction with a theoretical viscoelastic model. Isolated nuclei behaved as viscoelastic solid materials similar to the cytoplasm, but were three to four times stiffer than and nearly twice as viscous as the cytoplasm. Caille et al. [41] subjected endothelial cells to compression between glass microplates. This technique allowed measurement of the uniaxial force applied to the cell and the resulting deformation. Tests were also carried out with nuclei isolated from cell cultures by a chemical treatment. The elastic modulus of the cytoplasm was found to be on the order of 500 Pa for spread and round cells, whereas the elastic modulus of the endothelial nucleus was on the order of 5000 Pa for nuclei in the cell and on the order of 8000 Pa for isolated nuclei.

Taken as a whole, these results suggest that while the AVIC bulk mechanical stiffness is likely lower than that of the nucleus, these differences would not be expected to yield detectable differences in predicted NAR values. As mentioned above, it is more likely that other microarchitectural features of the AV leaflet ECM play a role in altering the local AVIC microenvironment. Additional high-resolution fibril-level studies are required to clarify this important mechanism of AV cellular deformation.

Potential Artifacts Due to Fixation. Chemical fixation processes are widely known to be capable of inducing morphological changes in cells and nuclei, such as shrinkage. In the current study we used NAR (i.e., the ratio of the nucleus major axis length to its minor axis length) to quantify nucleus shape. As a relative measure of nucleus shape, NAR does not depend on absolute nucleus size. Thus, NAR will be preserved so long as any shrinkage of the nucleus upon fixation is isotropic. In a recent study by Lei et al. [42], the aspect ratio of airway smooth muscle cell nuclei was used to quantify smooth muscle cell orientation. Lei et al. [42] concluded that fixation-related gross shrinkage of the tissue (trachea, in their case) was sufficiently isotropic to use the aspect ratio of the nucleus to measure cell orientation. In a classic paper by Skaer and Whytock [43], the effects of various fixatives on the morphology of the nucleus was reported. In contrast to other fixatives, glutaraldehyde (3%) was not observed to result in any swelling or shrinking of the nucleus [43]. In a more recent study by Blanc et al. [44], 0.6% glutaraldehyde was found to best preserve intracellular structures (including the nucleus), with little shrinkage or distortion compared with para-formaldehyde. Note that in the current study, 0.5% glutaraldehyde in PBS was used as

fixative. Moreover, our FE model predictions of NAR versus pressure closely matched experimental results at low pressure (i.e., 1 mm Hg), with increasing deviations as the pressure level increased. The close agreement between experimental results and FE model predictions at low pressure suggests that fixation has not affected NAR. The increasing deviations observed at higher pressure levels are likely due to fiber-compaction effects not accounted for by the FE model.

Wider Relevance of Current Study. A living, autologous tissue engineered heart valve (TEHV) may be capable of providing a more permanent solution for pulmonary valve (PV) replacement. Important with respect to the results of the current study, TEHV were able to function at least 20 weeks as PV substitutes in juvenile sheep, exhibiting a trilayered structure reminiscent of the native PV leaflet [45]. In-vitro studies have demonstrated that TEHV cultivated under static conditions displayed insufficient ECM formation for acute hemodynamic function. While more recent studies have relied on stem cells, a more slowly degrading scaffold and longer cultivation times to generate functional TEHV without the use of pulsatile flow [45], mechanical stimulation has nevertheless been demonstrated to play an important role in *accelerating* the process of TEHV tissue formation [46], and thus may play a critical role in future TEHV designs, in particular, within the context of rapidly degrading scaffolds.

A critical question in assessing and modeling the in-vitro TEHV tissue formation process will thus be how do the changes in the constituent cell population NAR relate to static and dynamic mechanotransductions in TEHV. As alluded to above, cells will generally respond to mechanical stimuli in a cell/tissue-dependent manner, and thus optimal biomechanical stimulation conditions determined for any one cell type may not be generally applicable. Our recent study using novel cell microintegrated scaffolds suggests that cellular deformations are comparable in magnitude to that found in the native valvular tissues, but respond differently to tissue-level stains due to the unique scaffold micromechanics [47]. Studies of native valve tissue responses can clearly help guide these studies, as they provide a base line toward which the TEHV remodeling process is likely attempting to emulate.

Summary. In the present study, the in-situ deformation of AVICs were investigated for the first time using porcine aortic valves fixed under 0–90 mm Hg TVPs. We observed large, consistent increases in AVIC NAR with TVP (e.g., from 1.8 at 0 mm Hg to 4.8 at 90 mm Hg transmural average), as well as pronounced layer specific variations. Relations to concomitant changes in collagen fiber alignment indicated that little AVIC deformation occurs with the large amount of fiber straightening via rotation that occurs at pressures below $\sim$1 mm Hg, followed by modest changes from 1–4 mm Hg, and finally substantial changes from 4 mm Hg to 90 mm Hg.

A tissue-level FE model was able to capture the qualitative response; however, it underpredicted AVIC deformation at higher TVPs. This suggested that additional micromechanical and fiber-compaction effects occur at high pressure levels. The results of this study form the basis of understanding TVP-mediated mechanotransduction within the AV and provide for the first time quantitative data correlating AVIC nuclei deformation with AV tissue microstructure and deformation. It should be noted that the entire AVIC deformation sequence occurs in $\leqslant$75 ms [48], the time required for the AV leaflet to fully close and reach full TVP. Moreover, AV leaflet strains are maintained for the entire diastolic phase (at least 300 ms). Thus, the AVIC deformations are also *maintained* for this period. However, it is unclear to what degree the AVIC's mechanobiological responses are "fine-tuned" for this unique micromechanical environment.

Acknowledgment

We are grateful to George C. Engelmayr, Jr. for many discussions and much valuable advice of the manuscript. Funding for this work was provided by NIH Grant Nos. HL 068816 and HL071814.

References

[1] Filip, D. A., Radu, A., and Simionescu, M., 1986, "Interstitial Cells of the Heart Valve Possess Characteristics Similar to Smooth Muscle Cells," Circ. Res., **59**(3), pp. 310–320.
[2] Taylor, P. M., Batten, P., Brand, N. J., Thomas, P. S., and Yacoub, M. H., 2003, "The Cardiac Valve Interstitial Cell," Int. J. Biochem. Cell Biol., **35**(2), pp. 113–118.
[3] Latif, N., Sarathchandra, P., Taylor, P. M., Antoniw, J., and Yacoub, M. H., 2005, "Molecules Mediating Cell-ECM and Cell-Cell Communication in Human Heart Valves," Cell Biochem. Biophys., **43**(2), pp. 275–287.
[4] Latif, N., Sarathchandra, P., Taylor, P. M., Antoniw, J., Brand, N., and Yacoub, M. H., 2006, "Characterization of Molecules Mediating Cell-Cell Communication in Human Cardiac Valve Interstitial Cells," Cell Biochem. Biophys., **45**(3), pp. 255–264.
[5] Sell, S., and Scully, R. E., 1965, "Aging Changes in the Aortic and Mitral Valves. Histologic and Histochemical Studies, With Observations on the Pathogenesis of Calcific Aortic Stenosis and Calcification of the Mitral Annulus," Am. J. Pathol., **46**, 345–365.
[6] Merryman, W. D., Youn, I., Lukoff, H. D., Krueger, P. M., Guilak, F., Hopkins, R. A., and Sacks, M. S., 2006, "Correlation Between Heart Valve Interstitial Cell Stiffness and Transvalvular Pressure: Implications for Collagen Biosynthesis," Am. J. Physiol. Heart Circ. Physiol., **290**(1), pp. H224–H231.
[7] Chester, A. H., Kershaw, J. D. B., Misfeld, M., Sievers, H.-H., and Yacoub, M. H., 2003, "Specific Regional and Directional Contractile Response of Aortic Cusp Tissue-Relevance to Valve Function," *Second Biennial Meeting of the Society for Heart Valve Disease*.
[8] Li, S., Van Den Diepstraten, C., D'Souza, S. J., Chan, B. M., and Pickering, J. G., 2003, "Vascular Smooth Muscle Cells Orchestrate the Assembly of Type I Collagen Via Alpha2beta1 Integrin, RhoA, and Fibronectin Polymerization," Am. J. Pathol., **163**(3), pp. 1045–1056.
[9] Sacks, M. S., Smith, D. B., and Hiester, E. D., 1998, "The Aortic Valve Microstructure: Effects of Transvalvular Pressure," J. Biomed. Mater. Res., **41**(1), pp. 131–141.
[10] Stella, J. A., and Sacks, M. S., 2007, "On the Biaxial Mechanical Properties of the Layers of the Aortic Valve Leaflet," ASME J. Biomech. Eng., **129**(5), pp. 757–766.
[11] Vesely, I., and Noseworthy, R., 1992, "Micromechanics of the Fibrosa and the Ventricularis in Aortic Valve Leaflets," J. Mol. Biol., **25**(1), pp. 101–113.
[12] Sacks, M. S., Smith, D. B., and Hiester, E. D., 1997, "ASmall Angle Light Scattering Device for Planar Connective Tissue Microstructural Analysis," Ann. Biomed. Eng., **25**(4), pp. 678–689.
[13] Sacks, M. S., 2004, "Small-Angle Light Scattering Methods for Soft Connective Tissue Structural Analysis," An invited chapter for the *Encyclopedia of Biomaterials and Biomedical Engineering*, G. E. Wnek and G. Bowlin, eds., Marcel Dekker, Inc., New York.
[14] Gloeckner, D. C., 2003, *Tissue Biomechanics of the Urinary Bladder Wall*, University of Pittsburgh, Pittsburgh, p. 258.
[15] Engelmayr, G. C., Jr., Rabkin, E., Sutherland, F. W., Schoen, F. J., Mayer, J. E., Jr., and Sacks, M. S., 2005, "The Independent Role of Cyclic Flexure in the Early In Vitro Development of an Engineered Heart Valve Tissue," Biomaterials, **26**(2), pp. 175–187.
[16] Huang, H. Y. S., 2004, "Micromechanical Simulations of Heart Valve Tissues," *Mechanical Engineering*, University of Pittsburgh, Pittsburgh, p. 258.
[17] Sugimoto, B., 2003, "Effects of Leaflet Stiffness on the Dynamic Motion of the Aortic Heart Valve," Master thesis, University of Pittsburgh.
[18] Mayne, A. S., Christie, G. W., Smaill, B. H., Hunter, P. J., and Barratt-Boyes, B. G., 1989, "An Assessment of the Mechanical Properties of Leaflets From Four Second-Generation Porcine Bioprostheses With Biaxial Testing Techniques," J. Thorac. Cardiovasc. Surg., **98**(2), pp. 170–180 (see comments).
[19] Billiar, K. L., and Sacks, M. S., 2000, "Biaxial Mechanical Properties of the Natural and Glutaraldehyde Treated Aortic Valve Cusp—Part I: Experimental Results," ASME J. Biomech. Eng., **122**(1), pp. 23–30.
[20] Kanit, T., Forest, S., and Galliet, I., 2003, "Determination of the Size of the Representative Volume Element for Random Composites: Statistical and Numerical Approach," Int. J. Solids Struct., **40**, pp. 3647–3679.
[21] Kouznetsova, V., Brekelmans, W. A. M., and Baaijens, F. P. T., 2001, "An Approach to Micro-Macro Modeling of Heterogeneous Materials," Arch. Technol., **27**(1), pp. 37–48.
[22] Billiar, K. L., and Sacks, M. S., 2000, "Biaxial Mechanical Properties of the Native and Glutaraldehyde-Treated Aortic Valve Cusp: Part II—A Structural Constitutive Model," ASME J. Biomech. Eng., **122**(4), pp. 327–335.
[23] Schmidt, D., and Sacks, M. S., 1998, "A Finite Element Implementation of a Structural Constitutive Model for Heart Valve Tissues for Generalized Deformation," J. Biomech., submitted.
[24] Theret, D. P., Levesque, M. J., Sato, M., Nerem, R. M., and Wheeler, L. T., 1988, "The Application of a Homogeneous Half-Space Model in the Analysis of Endothelial Cell Micropipette Measurements," ASME J. Biomech. Eng., **110**(3), pp. 190–199.
[25] Baer, A. E., Laursen, T. A., Guilak, F., and Setton, L. A., 2003, "The Micromechanical Environment of Intervertebral Disc Cells Determined by a Finite Deformation, Anisotropic, and Biphasic Finite Element Model," ASME J. Biomech. Eng., **125**(1), pp. 1–11.

[26] Baer, A. E., and Setton, L. A., 2000, "The Micromechanical Environment of Intervertebral Disc Cells: Effect of Matrix Anisotropy and Cell Geometry Predicted by a Linear Model," ASME J. Biomech. Eng., **122**(3), pp. 245–251.
[27] Liao, J., and Vesely, I., 2003, "A Structural Basis for the Size-Related Mechanical Properties of Mitral Valve Chordae Tendineae," J. Biomech., **36**(8), pp. 1125–1133.
[28] Knight, M. M., Ross, J. M., Sherwin, A. F., Lee, D. A., Bader, D. L., and Poole, C. A., 2001, "Chondrocyte Deformation Within Mechanically and Enzymatically Extracted Chondrons Compressed in Agarose," Biochim. Biophys. Acta, **1526**(2), pp. 141–146.
[29] Peeters, E. A., Bouten, C. V., Oomens, C. W., Bader, D. L., Snoeckx, L. H., and Baaijens, F. P., 2004, "Anisotropic, Three-Dimensional Deformation of Single Attached Cells Under Compression," Ann. Biomed. Eng., **32**(10), pp. 1443–1452.
[30] Screen, H. R., Lee, D. A., Bader, D. L., and Shelton, J. C., 2003, "Development of a Technique to Determine Strains in Tendons Using the Cell Nuclei," Biorheology, **40**(1–3), pp. 361–368.
[31] Merryman, W. D., Huang, H. Y., Schoen, F. J., and Sacks, M. S., 2006, "The Effects of Cellular Contraction on Aortic Valve Leaflet Flexural Stiffness," J. Biomech., **39**(1), pp. 88–96.
[32] Chester, A. H., Misfeld, M., and Yacoub, M. H., 2000, "Receptor-Mediated Contraction of Aortic Valve Leaflets," J. Heart Valve Dis., **9**(2), pp. 250–254.
[33] Silver, F. H., Kato, Y. P., Ohno, M., and Wasserman, A. J., 1992, "Analysis of Mammalian Connective Tissue: Relationship Between Hierarchical Structures and Mechanical Properties," J. Long Term Eff. Med. Implants, **2**(2–3), pp. 165–198.
[34] Cowin, S. C., 2000, "How is a Tissue Built?," ASME J. Biomech. Eng., **122**(6), pp. 553–569.
[35] Schoen, F., 1997, "Aortic Valve Structure-Function Correlations: Role of Elastic Fibers No Longer a Stretch of the Imagination," J. Heart Valve Dis., **6**, 1–6.
[36] Hilbert, S. L., Sword, L. C., Batchelder, K. F., Barrick, M. K., and Ferrans, V. J., 1996, "Simultaneous Assessment of Bioprosthetic Heart Valve Biomechanical Properties and Collagen Crimp Length," J. Biomed. Mater. Res., **31**(4), pp. 503–509.
[37] Scott, M. J., and Vesely, I., 1996, "Morphology of Porcine Aortic Valve Cusp Elastin," J. Heart Valve Dis., **5**(5), pp. 464–471.
[38] Merryman, W. D., Huang H.-Y. S., Schoen, F. J., and Sacks, M. S., 2006, "The Effects of Cellular Contraction on Aortic Valve Leaflet Flexural Stiffness," J. Biomech., **39**(1), pp. 88–96.
[39] Merryman, W. D., Liao, J., Parekh, A., Candiello, J. E., Lin, H., and Sacks, M. S., 2000, "Differences in Tissue Remodeling Potential of the Aortic and Pulmonary Heart Valve Interstitial Cells," Tissue Eng., **13**(9), pp. 2281–2290.
[40] Guilak, F., Tedrow, J. R., and Burgkart, R., 2000, "Viscoelastic Properties of the Cell Nucleus," Biochem. Biophys. Res. Commun., **269**(3), pp. 781–786.
[41] Caille, N., Thoumine, O., Tardy, Y., and Meister, J. J., 2002, "Contribution of the Nucleus to the Mechanical Properties of Endothelial Cells," J. Biomech., **35**(2), pp. 177–187.
[42] Lei, M., Ghezzo, H., Chen, M. F., and Eidelman, D. H., 1997, "Airway Smooth Muscle Orientation in Intraparenchymal Airways," J. Appl. Physiol., **82**(1), pp. 70–77.
[43] Skaer, R. J., and Whytock, S., 1976, "The Fixation of Nuclei and Chromosomes," J. Cell. Sci., **20**(1), pp. 221–231.
[44] Blanc, A., Tran-Khanh, N., Filion, D., and Buschmann, M. D., 2005, "Optimal Processing Method to Obtain Four-Color Confocal Fluorescent Images of the Cytoskeleton and Nucleus in Three-Dimensional Chondrocyte Cultures," J. Histochem. Cytochem., **53**(9), pp. 1171–1175.
[45] Sutherland, F. W., Perry, T. E., Yu, Y., Sherwood, M. C., Rabkin, E., Masuda, Y., Garcia, G. A., McLellan, D. L., Engelmayr, G. C., Jr., Sacks, M. S., Schoen, F. J., and Mayer, J. E., Jr., 2005, "From Stem Cells to Viable Autologous Semilunar Heart Valve," Circulation, **111**(21), pp. 2783–2791.
[46] Engelmayr, G. C., Jr., Sales, V. L., Mayer, J. E., Jr., and Sacks, M. S., 2006, "Cyclic Flexure and Laminar Flow Synergistically Accelerate Mesenchymal Stem Cell-Mediated Engineered Tissue Formation: Implications for Engineered Heart Valve Tissues," Biomaterials, **27**(36), pp. 6083–6095.
[47] Liao, J., Hong, Y., Merryman, W. D., Papworth, G. D., Wagner, W. R., and Sacks, M. S., 2007, "Cellular Deformations in Micro-Integrated Elastomeric Electrospun Scaffolds Under Biaxial Stretch," *2007 Society for Biomaterials Annual Meeting*, Chicago.
[48] Iyengar, A. K. S., Sugimoto, H., Smith, D. B., and Sacks, M. S., 2001, "Dynamic In Vitro Quantification of Bioprosthetic Heart Valve Leaflet Motion Using Structured Light Projection," Ann. Biomed. Eng., **29**(11), pp. 963–973.